Selective Gas Permeation in Defect-Engineered Bilayer Graphene

Jiaman Liu, Lei Jin, Frances I. Allen, Yang Gao, Penghong Ci, Feiyu Kang,* and Junqiao Wu*

Read Online

ACCESS | Metrics & More | Article Recommendations | Supporting Information

ABSTRACT: Defective graphene holds great potential to enable the permeation of gas molecules at high rates with high selectivity due to its one-atom thickness and resultant atomically small pores at the defect sites. However, precise control and tuning of the size and density of the defects remain challenging. In this work, we introduce atomic-scale defects into bilayer graphene via a decoupled strategy of defect nucleation using helium ion irradiation followed by defect expansion using hydrogen plasma treatment. The cotreated membranes exhibit high permeability and simultaneously high selectivity compared to those singly treated by ion irradiation or hydrogen plasma only. High permeation selectivity values for H_2/N_2 and H_2/CH_4 of 495 and 877, respectively, are achieved for optimally cotreated membranes. The method presented can also be scaled up to prepare large-area membranes for gas separation, e.g., for hydrogen purification and recovery from H_2/CH_4 and H_2/N_2 mixtures.

KEYWORDS: bilayer graphene, gas permeation, ion irradiation, defect engineering
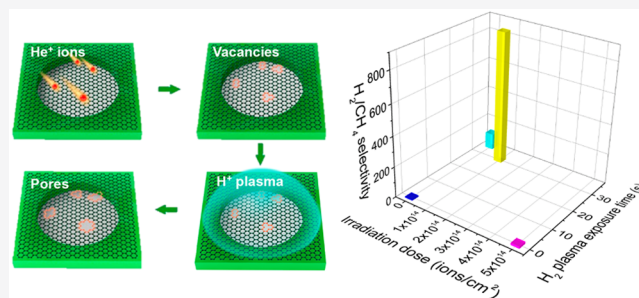
Conventional, distillation-based gas separation technology in the petrochemical industry is energy intensive and environmentally unfriendly. In contrast, the rapidly growing field of membrane technology offers new strategies for sustainable gas separation, providing modularity, scalability, compactness, and high energy efficiency. Being atomically thin, two-dimensional (2D) materials provide a unique opportunity to realize high separation capacity together with excellent selectivity as a new class of membrane materials. However, it was not until 2008, when the impermeability of graphene to helium and other gases was reported by Bunch et al.,[1] that gas sieving through atomically thin membrane became a viable option.

Soon after, a large number of theoretical studies explored the transport of different gas molecules through perforated 2D materials, albeit with significantly different levels of permeance and selectivity for different gases.[2] One of the most straightforward methods to perforate graphene is through the introduction of point defects, the size of which can control the permeability in an exponential manner.[3] In addition, for certain pore sizes, gaseous molecules that are more adsorptive tend to have higher permeation rates than less adsorptive ones.[4] For example, comparing two adsorptive gases, e.g., CO_2 and CH_4, interacting with nanoporous graphene, a trade-off exists between CO_2 permeance and CO_2/CH_4 selectivity. Theoretically, functionalization of the pore edge with H, N, F, and O atoms is also expected to alter the pore's gas transport properties.[5] It is worth noting that experimental research demonstrating the effect of pore termination groups on the behavior of gas transport in defective graphene is still lacking.

As the permeance of a membrane is inversely proportional to its thickness, nanoporous, atomically thin graphene presents the possibility to combine high permeability and selectivity beyond the Robeson upper bound.[2] Several studies in the past have explored various defect engineering techniques in 2D materials, including hydrogen plasma irradiation,[6] oxygen plasma irradiation,[6−8] focused ion beam irradiation,[7,9,10] thermal annealing,[10] UV/ozone treatment,[11] or a combination of these.[6,7,10] Koening et al.[11] showed that a bilayer graphene (BLG) balloon can exhibit different gas molecule cutoff sizes as verified by selective transport of various gases. Such different cutoff sizes coupled with a high selectivity of over 4 orders of magnitude may be ascribed to a different chemical termination formed during the oxidative etching nanopore fabrication process.

In this work, we explore two defect engineering techniques of graphene for gas separation, namely, helium (He^+) ion irradiation and hydrogen (H_2) plasma etching. The techniques are applied separately and in a combined approach. In this two-step process, He^+ ion irradiation is first used to introduce point defects, and then, H_2 plasma treatment is used to grow atomic-scale pores into a BLG membrane (Figure 1a). While the former is effective in generating carbon vacancies at controlled
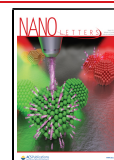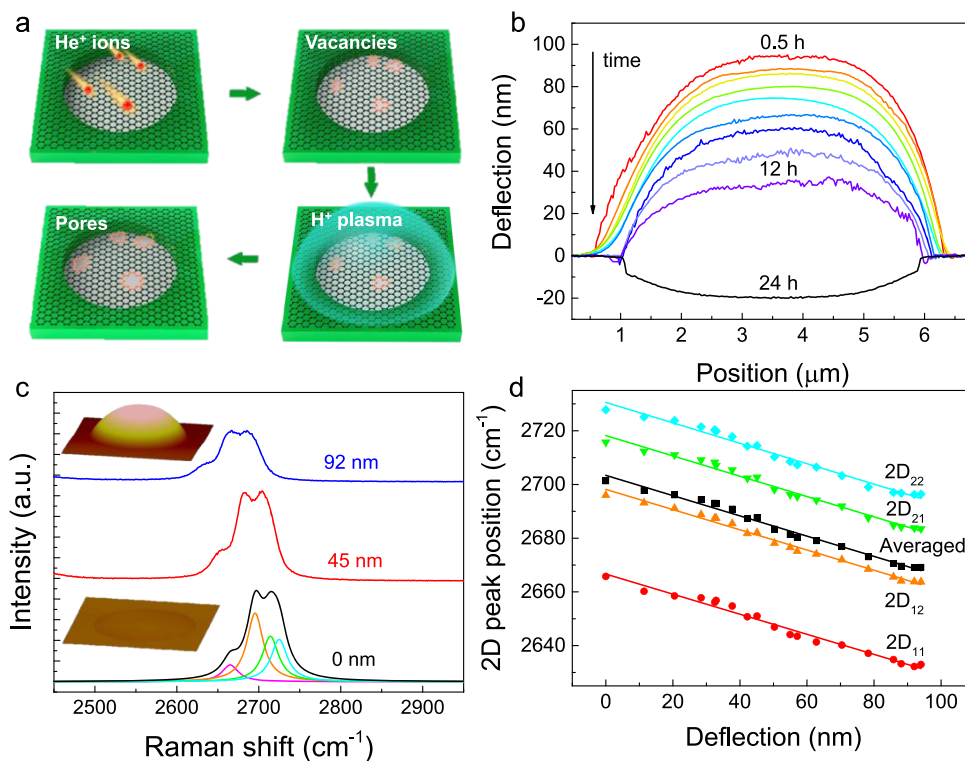
Figure 1. Defect generation and AFM and Raman characterization of the deflection of the BLG balloon. (a) Schematic of the decoupled defect nucleation and pore expansion process. (b) AFM line traces taken across the center of a BLG membrane microcavity over a period of 24 h when exposed to ambient air. The BLG microcavity inflated with H_2 shows a gradually reducing membrane deflection. (c) Raman spectra of the inflated BLG membrane with different levels of deflection determined by AFM. The two insets show the AFM images of the BLG membrane corresponding to 0 and 92 nm deflection. (d) Raman shifts of the 2D peaks and their average as a function of deflection.

densities, the subsequent plasma treatment allows for controlled enlargement of the irradiation-generated vacancies, since radicals in the plasma are easily chemisorbed at locations with dangling bonds.[12] It is shown that optimal gas molecule sieving properties are achieved when the two defect engineering techniques work sequentially but synergistically to first nucleate and then grow point defects in graphene.

The BLG membranes for this study are directly exfoliated onto an array of disk-shaped microcavities pre-etched in an oxidized silicon wafer with 300 nm silicon oxide on top (Figure S1). The sample is first placed in a vacuum chamber (pressure ∼0.05 Torr) for 4 h to evacuate the air sealed in the microcavities. The chamber is then filled with the test gas (He, H_2, N_2, or CH_4) overpressured at 2000−3000 Torr for 48 h, such that the molecules of the test gas diffuse into the microcavities and fully equilibrate with the outside overpressure. Once taken out of the chamber to ambient air, the BLG membrane sealing each microcavity bulges up and becomes a spherical cap-shaped balloon due to the pressure difference between the inside and outside of the balloon. The height of the spherical cap gradually reduces with time, reflecting leakage of the test gas molecules through the BLG membrane.

Before perforation, these pristine BLG balloons are almost impermeable to all tested gases. Figure 1b shows a series of atomic force microscopy (AFM) line traces across the center of a single BLG membrane cavity taken over a period of 24 h. The initial upward deflection is $\delta \sim 96$ nm and decreases slowly over time, indicating a slow leak of H_2 from the microcavity through the pristine BLG. For such a clamped circular membrane, the molecular flux, dn/dt, leaking out of

the overpressurized "blister" is proportional to $d\delta/dt$, where n is the number of moles of gas molecules sealed in the microcavity, and t is time (Note S1 in the Supporting Information).[11] When the BLG balloon is deflected to a certain height δ, the tensile strain raises the interatomic distance in the BLG, leading to a softening of the Raman modes.[13] Figure 1c shows the 2D Raman peak position taken from the center of the BLG balloon at different deflections. Raman peak position plotted as a function of the deflection yields a linear relationship with an averaged slope of -0.37 cm^{-1}/nm as shown in Figure 1d. This is verified in both pristine and low-dose irradiation-only BLG (irradiated with 5×10^{13} and 5×10^{14} ions/cm^2). Therefore, by measuring the evolution of the 2D Raman peak position of the BLG membrane (also referred to as the Raman peak position shift rate) over time t, the gas leak rate across the BLG membrane can be calculated.

The effect of He$^+$ ion irradiation on freestanding BLG is first investigated. For the pristine BLG membrane, there is no noticeable D or D′ peak, indicating that the material is largely defect-free (Figure 2a). For a low irradiation dose of only 5×10^{13} ions/cm^2, a small D peak is observed. As the irradiation dose continues to increase, both D and D′ peaks become more prominent, and the intensity of the 2D peak gradually reduces. Irradiation at a dose of 5×10^{15} ions/cm^2 greatly disorders the graphene lattice; the 2D peak is hardly visible and the G peak starts to overlap with the D′ peak. The evolution of defects in graphene treated by ion irradiation only is known to follow a three-stage amorphization process (Note S2 in Supporting Information) as proposed by Ferrari et al.,[14] and it can be characterized by the intensity ratio between the D and G peaks. As shown in Figure 2b, I_D/I_G first increases and then
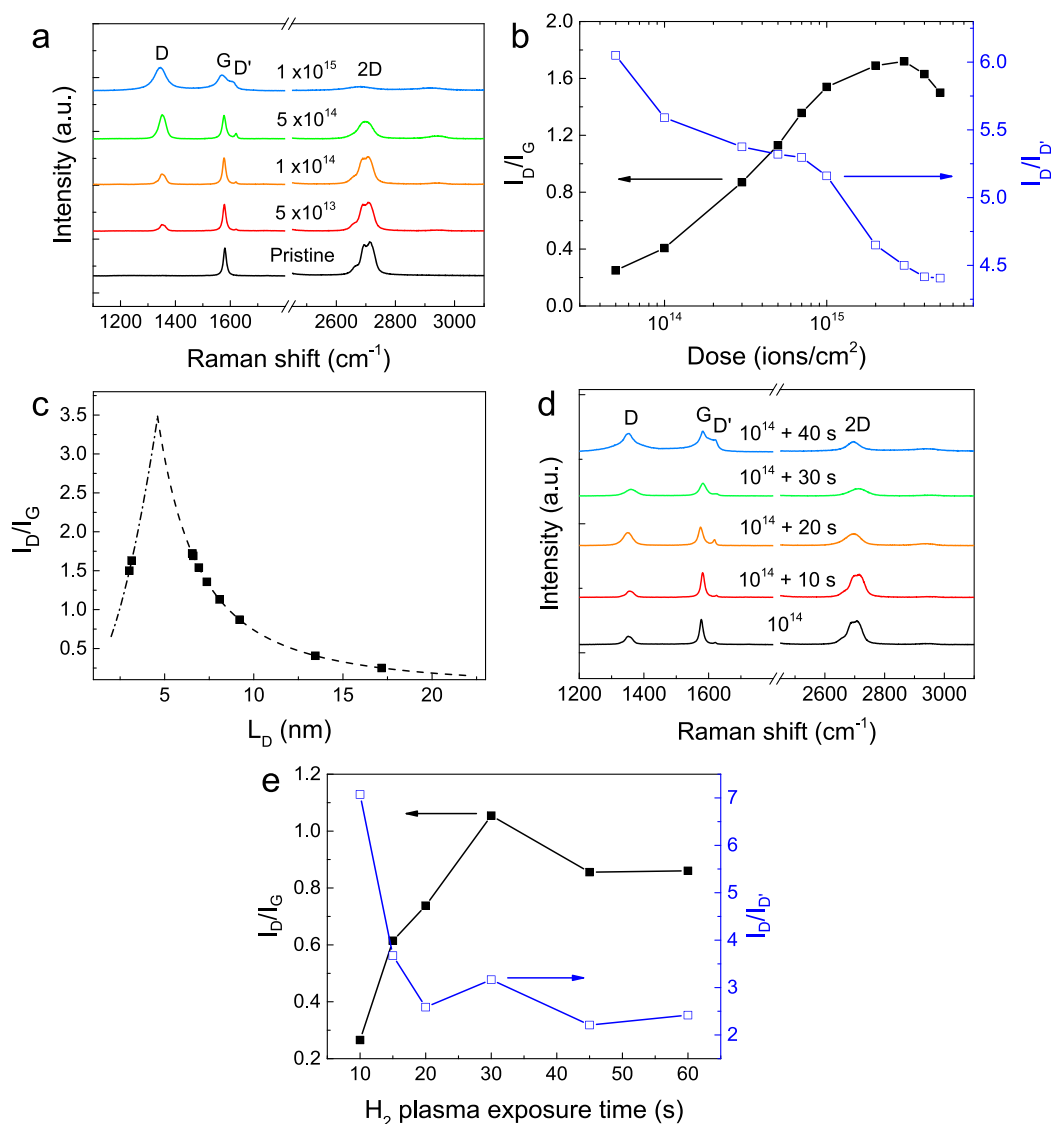
Figure 2. Characterization of a BLG membrane treated with ion irradiation only and cotreated using ion irradiation followed by plasma exposure. (a) Evolution of 2D, D′, G, and D Raman peaks as a function of He$^+$ irradiation dose. (b) Corresponding evolution of peak intensity ratios I_D/I_G and $I_D/I_{D'}$ from panel a versus irradiation dose. (c) Corresponding intensity ratio I_D/I_G versus defect distance L_D. The dashed line is for a fit according to ref 15. (d) Evolution of 2D, D′, G, and D peaks as a function of H$_2$ plasma treatment time following He$^+$ irradiation at a dose of 10^{14}/cm^2. (e) Corresponding intensity ratios I_D/I_G and $I_D/I_{D'}$ from panel d versus plasma treatment time.

decreases after reaching a maximum, where the maximum and behavior afterward are indicative of the onset of stage two in the amorphization process. The gradual broadening of the D and G peaks (Figure 2a) is also consistent with this amorphization trajectory. The defect type is generally reflected by the $I_D/I_{D'}$ ratio: sp^3-type defects have $I_D/I_{D'} > 7$ while vacancy-type defects have $I_D/I_{D'} < 7$. The $I_D/I_{D'}$ ratio in Figure 2b ranges from ∼6 for 5×10^{13} ions/cm^2 to ∼4.5 for 5×10^{15} ions/cm^2. These values suggest that vacancy-like defects are dominantly generated in the irradiation process for the doses investigated. Using the equation adopted from ref 15

$$L_D^2 \ (\text{nm}^2) = (1.8 \pm 0.5) \times 10^{-9} \lambda_L^4 \left(\frac{I_D}{I_G} \right)^{-1}$$

where λ_L is the laser wavelength used for the Raman spectroscopy, the relationship between I_D/I_G and the average distance between defects (L_D) can be obtained (Figure 2c). With a decreasing L_D, the defect density n_D increases

accordingly, from 1.08×10^{11} cm^{-2} for 5×10^{13} ions/cm^2 to 3.49×10^{12} cm^{-2} for 5×10^{15} ions/cm^2 (also see Table S1). These values are comparable to values reported in the literature,[8] but with predominantly isolated vacancy-type defects in our case.

Next, to investigate the effect of the two-step engineering approach for generating atomic-scale defects, a BLG membrane is first irradiated at a fixed dose of 1×10^{14} ions/cm^2 (estimated n_D of 1.76×10^{11} cm^{-2}) and then exposed to H$_2$ plasma for varying amounts of time. Figure 2d shows the evolution of the Raman spectra of such a cotreated BLG membrane as a function of plasma exposure time. It is important to note that the interaction between graphene and hydrogen radicals generally involves two processes, namely, hydrogenation (stage 1), then amorphization and carbon ablation (stage 2).[16] During the hydrogenation process, hydrogen atoms are bonded to carbon atoms by breaking the conjugated π system. When hydrogen coverage increases
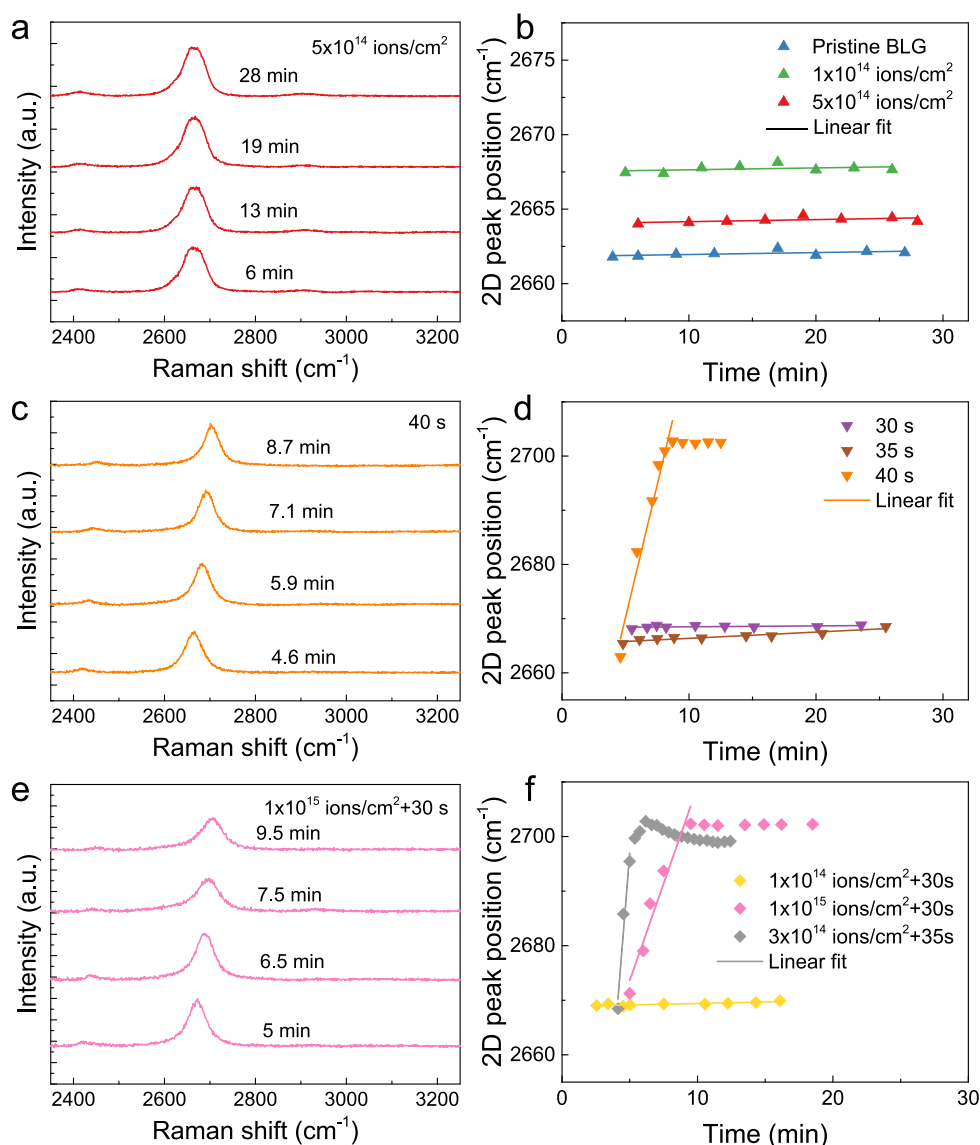
Figure 3. N_2 permeation results for the three perforated BLG membrane types. (a) Evolution of Raman spectra for a BLG balloon upon N_2 gas permeation after ion irradiation at a dose of 5×10^{14} ions/cm^2. (b) Corresponding 2D peak position evolution for the irradiation-only treated BLG balloon. (c) Evolution of Raman spectra for a 40 s plasma-only treated BLG balloon upon N_2 gas permeation. (d) Corresponding 2D peak evolution for the plasma-only treated BLG balloon. (e) Evolution of Raman spectra for a BLG balloon cotreated first by irradiation with 1×10^{15} ions/cm^2 followed by 30 s exposure to plasma. (f) Corresponding 2D peak evolution for the cotreated BLG balloon.

further, graphene amorphization via C−C σ bond breaking and subsequent carbon ablation also occurs. In Figure 2d, after 15 s of plasma exposure, an obvious D′ peak appears, and with continued plasma exposure, $I_{D'}$ increases even further, indicating continuation of the stage 1 hydrogenation process. The transition from stage 1 to stage 2 is usually indicated by reaching a maximum value of I_D/I_G.[17] Here, this transition occurs for a plasma exposure time of 30 s, with the I_D/I_G ratio reaching a maximum value of 1.05 (Figure 2e). Further exposure (>30 s) decreases the I_D/I_G ratio. This trend reflects the behavior that, for longer plasma exposure times, sp^3 defects and porosity are generated and increase in density, thus reducing the density of ordered six-atom rings in the graphene lattice. As the ratio $I_D/I_{D'}$ is smaller than 3.5 with long plasma exposure times (>20 s), boundary-like defects (i.e., enlarged vacancy-like defects) dominate.[18] For comparison, the BLG membrane is also treated with plasma only without the He$^+$ ion irradiation step (Figure S2). The resulting gas transport

properties of the ion irradiation-only, plasma-only, cotreated BLG membrane, and a control as-exfoliated BLG membrane, are compared in the following.

For the control experiment, the gas transport properties of as-exfoliated BLG balloons ("pristine BLG") are evaluated using a modified pressurized blister test, in which Raman spectroscopy is used to indirectly monitor the evolution of the deflection. In Figure 3a,b and Figure S3, it is obvious that, within the shown period of time, almost no Raman shift is observed for pristine BLG balloons, as well as for those only irradiated at low doses of 5×10^{13}, 1×10^{14}, and 5×10^{14} ions/cm^2. The deflections of each BLG membrane are also confirmed by AFM, which shows a height that is independent of time for the first hour after retrieval from the pressure chamber (Figure S4). After pressurization for a second time, a similar lack of deflation of the BLG balloon over the 1 h time frame is observed. As the blisters themselves may possibly leak through the SiO$_2$ substrate surface, or through the BLG−SiO$_2$
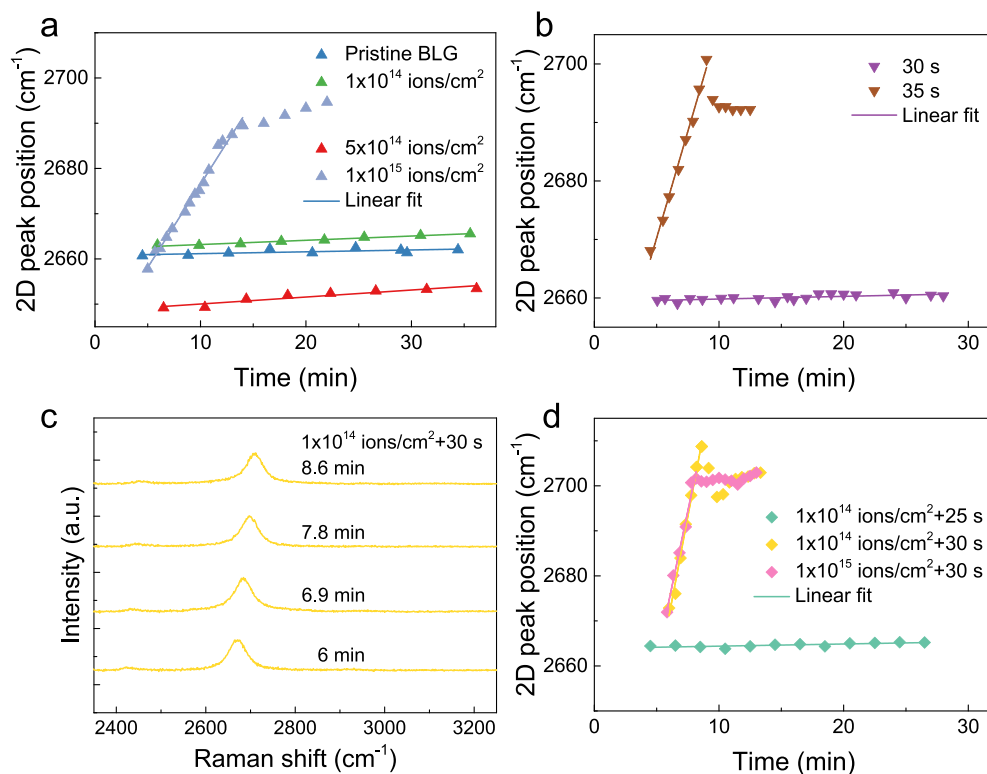
Figure 4. H_2 permeation results for the three perforated BLG membrane types. (a) Raman 2D peak evolution for irradiation-only BLG balloons. (b) Raman 2D peak evolution for plasma-only BLG balloons. (c) Evolution of Raman spectra for BLG balloon cotreated with 1×10^{14} ions/cm^2 and 30 s plasma exposure. (d) Corresponding 2D peak evolution for cotreated BLG balloons.

interface, the observed extremely slow deflation in these pristine and low-dose irradiation-only BLG membranes indicate either impermeability or very weak permeation through these pathways.

Turning to the permeation results for BLG membranes treated with the plasma-only method using a plasma exposure time of 30–35 s (Figure 3d), no significant Raman shift is observed for up to ~30 min. This is also confirmed by AFM measurements. All the BLG balloons remain inflated within 1 h after retrieval from the pressure chamber, indicative of a very slow leak rate, if any, through the SiO_2. However, for the BLG balloon with 40 s of plasma exposure (Figure 3c,d), a gradual blue-shift of the Raman spectra over time is observed, indicative of a fast leak rate. The 2D peak position shift rate is ~9.81 cm^{-1}/min. With a conversion of this value to a deflection change rate using the averaged conversion factor from Figure 1d, the normalized dn/dt is calculated to be ~4 × 10^{-24} mol s^{-1} Pa^{-1}. After the Raman shift stabilizes and remains unchanged for ~30 min, AFM measurements are carried out and reveal that the balloon becomes flat, indicating that the encapsulated gas molecules have leaked out of the BLG balloon and the pressure reaches equilibrium between the inside and outside of the membrane. For an even longer exposure time to the plasma, the BLG membrane becomes severely damaged and thus cannot be inflated.

In the case of the cotreated BLG balloons, using an irradiation dose of 1×10^{14} ions/cm^2 followed by plasma exposure for 30 s (denoted as "1×10^{14} ions/cm^2 + 30s" hereafter), no 2D peak shift is observed (Figure 3f). In the 1×10^{15} ions/cm^2 + 30 s sample, however, the 2D Raman peak gradually blue-shifts to a constant position within 10 min (Figure 3e,f). The 2D peak shift rate for this sample is ~7 × 10

cm^{-1}/min, giving a leak rate of ~3 × 10^{-24} mol s^{-1} Pa^{-1}. Another sample with 3 × 10^{14} ions/cm^2 + 35 s treatment has a very high Raman peak shift rate of ~30.73 cm^{-1}/min, corresponding to a leak rate of ~1 × 10^{-23} mol s^{-1} Pa^{-1}. Table S2 summarizes the N_2 leak rates for all the conditions employed to treat the BLG membranes. The area-normalized dn/dt for pristine BLG is consistent with those reported in ref 11. The plasma-only sample treated for 35 s has a leak rate around an order of magnitude higher than the pristine sample, while the plasma-only sample treated for 40 s exceeds the leak rate of the pristine sample by 3 orders of magnitude.

Using the same experimental approach, the H_2 leak rates for irradiation-only, plasma-only, and cotreated BLG balloons are also investigated. It should be noted that we primarily used the same samples for the measurements of different gases unless the samples were broken between measurements, in which case we prepared new samples. For the irradiation-only samples (Figure 4a), it is clear that the Raman 2D peak position shift rate gradually increases with increasing treatment dose, reaching 3.68 cm^{-1}/min in the 1×10^{15} ions/cm^2 sample. In the case of the plasma-only samples, a plasma exposure of 35 s makes the sample permeable to H_2 with relatively fast leak rates (Figure 4b). Interestingly, although both the 1×10^{14} ions/cm^2 sample and the 30 s plasma-only treated sample show minute 2D peak shifts, the cotreated BLG (1×10^{14} ions/cm^2 + 30 s) is capable of leaking out most H_2 molecules within 10 min, as shown in Figure 4c. In Figure 4d, the 1 × 10^{14} ions/cm^2 + 30 s sample is found to be the threshold condition for H_2 sieving because a shorter plasma treatment time leads to almost no Raman shift whereas a higher irradiation dose has a relatively high Raman shift rate. It should be noted that the cotreated BLG (i.e., 1×10^{14} ions/cm^2 + 30
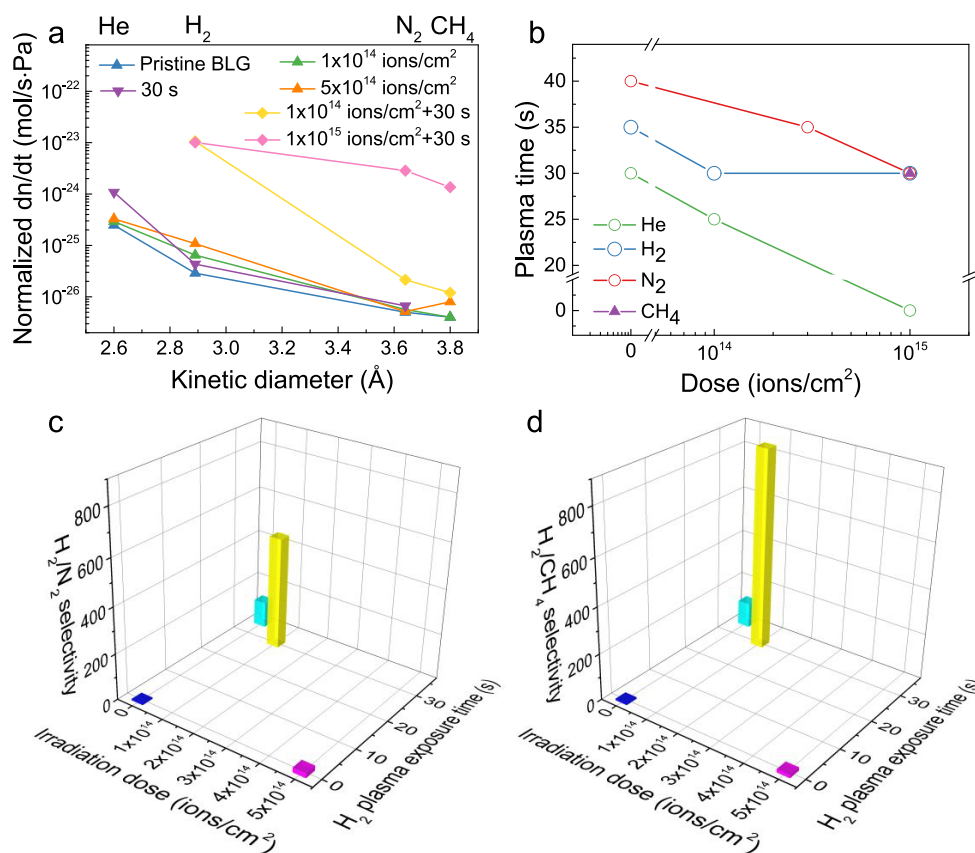
Figure 5. Figure of merit for molecule permeation through the various BLG membranes. (a) Summary of measured leak rates for the irradiation-only, plasma-only, cotreated, and pristine BLG balloons. (b) Permeance map of He, H_2, N_2, and CH_4 molecules as a function of irradiation dose and plasma treatment time. The data points represent the treatment condition when the permeation becomes equal to twice that of the pristine sample. (c) Selectivity of H_2/N_2 and (d) H_2/CH_4 for BLG balloons with nanopores created using the treatments as labeled.

s) has a H_2 leak rate that is around 250 times higher than that of the plasma-only treated sample (i.e., 30 s plasma treatment) as shown from Table S3.

Similar to the N_2 case, a three-orders-of-magnitude increase in the H_2 leak rate is found in the 1×10^{15} ions/cm^2 + 30 s sample, reaching $\sim 1 \times 10^{-23}$ mol s^{-1} Pa^{-1}. Surprisingly, the 1×10^{14} ions/cm^2 + 30 s sample, which is almost impermeable to N_2, has a H_2 leak rate comparable to that of the 1×10^{15} ions/cm^2 + 30 s sample. This selectivity between H_2 and N_2 suggests that the pore sizes introduced into the BLG membrane for this cotreatment condition are comparable to the kinetic diameter of H_2 (2.89 Å) and, hence, separate molecules larger than this size (e.g., N_2) from those below this size. The measured leak rate can be compared to the theoretical results from Blankenburg et al.,[19] in which H_2 mainly leaks through hydrogen-terminated pores consisting of a single missing benzene ring, and the leak rate was calculated to be on the order of 1×10^{-23} mol s^{-1} Pa^{-1}, similar to our result.

We also investigate the permeation of He and CH_4. For He, with a kinetic size smaller than H_2, the leak rate is also found to gradually increase with an increasing irradiation dose, with the 1×10^{15} ions/cm^2 sample showing a Raman peak shift rate of ~ 1.78 cm^{-1}/min (Figure S5a, Table S4). This value is lower than the H_2 leak rate for the same treatment condition, indicative of a smaller energy barrier for H_2 permeation than for He. This may result from an increased amount of rippling of the BLG membrane that may occur at the high doses of $1 \times$

10^{15} ions/cm^2; in related work, ripples have been shown to have a catalytic effect on the dissociation of molecular hydrogen, which in turn results in non-negligible permeation of hydrogen.[20] In addition, a plasma-only sample treated using a shorter exposure time of 30 s (compared to 35 s for H_2 and 40 s for N_2) opens up pores for He to diffuse through. The leak rate of this membrane is $\sim 1.09 \times 10^{-24}$ mol s^{-1} Pa^{-1}, which is around an order of magnitude higher than the pristine membrane (Figure S5a, Table S4). In contrast, CH_4, the largest molecule investigated, remains impermeable in most of the BLG membranes, becoming permeable only in the 1×10^{15} ions/cm^2 + 30 s sample (Figure S5b, Table S5).

In Figure 5a, the leak rates of the different gas molecules versus their kinetic diameter are plotted for the various BLG membranes. In general, the leak rates decrease with increasing kinetic diameter of the gas molecule, both for the pristine and the defective (treated) BLG samples. Low leakage is observed in the low-dose irradiation-only membranes. Plasma exposure of 30 s enables the permeation of He while blocking the transport of other, larger gas molecules. Thus, the kinetic diameter cutoff size in this membrane is ~ 2.6 Å. The BLG membrane with 1×10^{14} ions/cm^2 + 30 s treatment also allows the permeation of H_2 while prohibiting the permeation of N_2 and CH_4. Thus, the kinetic diameter cutoff size in the 1×10^{14} ions/cm^2 + 30 s membrane can be inferred to be ~ 2.89 Å. The effectiveness of the various treatment combinations for the permeability of the four different gases tested is summarized in Figure 5b, where the data points represent the treatment

condition for which the permeation becomes equal to twice that of the pristine sample. For gas molecules with smaller kinetic diameters (i.e., He), it becomes clear that a shorter duration of plasma exposure is needed in order to generate suitable pores. In addition, it is found that the two-step ion irradiation plus plasma treatment defect engineering approach is more effective for permeating H_2 and the larger-diameter gas molecules, albeit with different values of gas permeance.

The permeation selectivity results for H_2/N_2 and H_2/CH_4 are summarized in Figure 5c,d, respectively. Pristine BLG shows very low selectivity for H_2/N_2 and H_2/CH_4 (in blue). A low irradiation dose, i.e., 5×10^{14} ions/cm^2 (in purple), results in approximately a 4-fold increase in H_2 permeance (from 2.73×10^{-16} to 1.02×10^{-15} mol m^{-2} s^{-1} Pa^{-1}), while also increasing the H_2/N_2 selectivity (5.8 to 20.9) and the H_2/CH_4 selectivity (7.2 to 13.5). In terms of the plasma-only treatment (in cyan), a 35 s exposure results in an increase in H_2 permeance of around 2 orders of magnitude, i.e., 4.97×10^{-14} mol m^{-2} s^{-1} Pa^{-1}. The resultant H_2/N_2 and H_2/CH_4 selectivities show approximately 20-fold and 15-fold increases compared to the pristine samples, reaching 113 and 109, respectively. Significantly, we observed ultrahigh H_2/N_2 selectivity of 495 and H_2/CH_4 selectivity of 877 in the 1×10^{14} ions/cm^2 + 30 s cotreatment case (in yellow), while maintaining a high permeance of 1.06×10^{-13} mol m^{-2} s^{-1} Pa^{-1} for H_2. This selectivity is much higher than most reported values in the literature and could be attributed to the suitable pore size and hydrogenated edges created in the cotreated 1×10^{14} ions/cm^2 + 30 s membrane, which would largely reduce the H_2 penetration barrier during the molecular diffusion process as recently proposed in the literature.[20]

In conclusion, a two-step fabrication process of decoupling defect nucleation and expanding the pore is shown to be advantageous for precisely generating atomic pores of the desired diameters and densities in BLG membranes. Bilayer graphene that is treated with He$^+$ ion irradiation only permeates He and H_2 molecules at a relatively low rates, whereas plasma-only treatment leads to high permeation rates for H_2 and N_2. In contrast, by sequentially combining He$^+$ ion irradiation with H_2 plasma exposure at optimal processing conditions, H_2-permeating BLG membranes with high H_2/N_2 selectivity can be obtained. These findings indicate that nanopores in BLG membranes could be created with optimal sizes for effective sieving of different gas molecules, of particular relevance in the field of hydrogen recovery from refinery off-gas streams. These results also open up new avenues for developing precisely controlled nanoporous 2D membranes for controlled interactions with ions and molecules.

ASSOCIATED CONTENT

Supporting Information

The Supporting Information is available free of charge at https://pubs.acs.org/doi/10.1021/acs.nanolett.0c04989.

> More details for the experimental setup and measurement system; Notes S1 and S2, Figures S1−S5, Tables S1−S5, and references; optical image of BLG exfoliated onto an SiO$_2$(300 nm)/Si wafer; Raman spectra of H_2 plasma treated BLG; evolution of Raman spectra for ion irradiated BLG; AFM images of BLG balloon; H_2 and CH$_4$ permeance results; experimental values for L_D and

n_D; N$_2$ leak rates; H_2 leak rates; He leak rates; and CH$_4$ leak rates (PDF)

AUTHOR INFORMATION

Corresponding Authors

Feiyu Kang − *Environmental Science and New Energy Technology Engineering Laboratory, Shenzhen Geim Graphene Center (SGGC), and Tsinghua-Berkeley Shenzhen Institute (TBSI), Institute of Materials Research and Shenzhen Geim Graphene Center (SGGC), Shenzhen International Graduate School (SIGS), and Laboratory of Advanced Materials, School of Materials Science and Engineering, Tsinghua University, Shenzhen 518055, China*; Email: fykang@sz.tsinghua.edu.cn

Junqiao Wu − *Department of Materials Science and Engineering, University of California, Berkeley, California 94720, United States; Materials Sciences Division, Lawrence Berkeley National Laboratory, Berkeley, California 94720, United States;* orcid.org/0000-0002-1498-0148; Email: wuj@berkeley.edu

Authors

Jiaman Liu − *Environmental Science and New Energy Technology Engineering Laboratory, Shenzhen Geim Graphene Center (SGGC), and Tsinghua-Berkeley Shenzhen Institute (TBSI), Tsinghua University, Shenzhen 518055, China; Department of Materials Science and Engineering, University of California, Berkeley, California 94720, United States*

Lei Jin − *Department of Materials Science and Engineering, University of California, Berkeley, California 94720, United States; Materials Sciences Division, Lawrence Berkeley National Laboratory, Berkeley, California 94720, United States*

Frances I. Allen − *Department of Materials Science and Engineering, University of California, Berkeley, California 94720, United States; National Center for Electron Microscopy, Molecular Foundry, Lawrence Berkeley National Laboratory, Berkeley, California 94720, United States*

Yang Gao − *Department of Materials Science and Engineering, University of California, Berkeley, California 94720, United States; Department of Engineering Mechanics, Zhejiang University, Hangzhou 310027, China*

Penghong Ci − *Department of Materials Science and Engineering, University of California, Berkeley, California 94720, United States; Materials Sciences Division, Lawrence Berkeley National Laboratory, Berkeley, California 94720, United States*

Complete contact information is available at:
https://pubs.acs.org/10.1021/acs.nanolett.0c04989

Author Contributions

All authors discussed and contributed to the preparation of the manuscript.

Notes

The authors declare no competing financial interest.

were performed at Berkeley Marvall NanoLab at CITRIS, at the University of California, Berkeley.

ABBREVIATIONS

2D: two-dimensional
BLG: bilayer graphene
AFM: atomic force microscopy

REFERENCES

(1) Bunch, J. S.; Verbridge, S. S.; Alden, J. S.; van der Zande, A. M.; Parpia, J. M.; Craighead, H. G.; McEuen, P. L. Impermeable atomic membranes from graphene sheets. *Nano Lett.* **2008**, *8* (8), 2458−2462.

(2) Wang, L.; Boutilier, M. S. H.; Kidambi, P. R.; Jang, D.; Hadjiconstantinou, N. G.; Karnik, R. Fundamental transport mechanisms, fabrication and potential applications of nanoporous atomically thin membranes. *Nat. Nanotechnol.* **2017**, *12* (6), 509−522.

(3) Leenaerts, O.; Partoens, B.; Peeters, F. M. Graphene: A perfect nanoballoon. *Appl. Phys. Lett.* **2008**, *93* (19), 193107.

(4) Du, H.; Li, J.; Zhang, J.; Su, G.; Li, X.; Zhao, Y. Separation of hydrogen and nitrogen gases with porous graphene membrane. *J. Phys. Chem. C* **2011**, *115* (47), 23261−23266.

(5) Drahushuk, L. W.; Strano, M. S. Mechanisms of gas permeation through single layer graphene membranes. *Langmuir* **2012**, *28* (48), 16671−16678.

(6) Xie, G.; Yang, R.; Chen, P.; Zhang, J.; Tian, X.; Wu, S.; Zhao, J.; Cheng, M.; Yang, W.; Wang, D.; He, C.; Bai, X.; Shi, D.; Zhang, G. A general route towards defect and pore engineering in graphene. *Small* **2014**, *10* (11), 2280−4.

(7) Boutilier, M. S. H.; Jang, D.; Idrobo, J. C.; Kidambi, P. R.; Hadjiconstantinou, N. G.; Karnik, R. Molecular Sieving Across Centimeter-Scale Single-Layer Nanoporous Graphene Membranes. *ACS Nano* **2017**, *11* (6), 5726−5736.

(8) Zhao, J.; He, G.; Huang, S.; Villalobos, L. F.; Bassas, H.; Agrawal, K. V.; Dakhchoune, M. Etching gas-sieving nanopores in single-layer graphene with an angstrom precision for high-performance gas mixture separation. *Sci. Adv.* **2019**, *5* (eaav1851), 9.

(9) Thiruraman, J. P.; Dar, S. A.; Das, P. M.; Hassani, N.; Neek-Amal, M.; Keerthi, A.; Drndic, M.; Radha, B. Gas flow through atomic-scale apertures. *Sci. Adv.* **2020**, *6*, eavc7927.

(10) Schlichting, K.-P.; Poulikakos, D. Selective etching of graphene membrane nanopores: from molecular sieving to extreme permeance. *ACS Appl. Mater. Interfaces* **2020**, *12* (32), 36468−36477.

(11) Koenig, S. P.; Wang, L.; Pellegrino, J.; Bunch, J. S. Selective molecular sieving through porous graphene. *Nat. Nanotechnol.* **2012**, *7* (11), 728−732.

(12) Mehedi, H. A.; Ferrah, D.; Dubois, J.; Petit-Etienne, C.; Okuno, H.; Bouchiat, V.; Renault, O.; Cunge, G. High density H2 and He plasmas: Can they be used to treat graphene? *J. Appl. Phys.* **2018**, *124* (12), 125304.

(13) Mohiuddin, T. M. G.; Lombardo, A.; Nair, R. R.; Bonetti, A.; Savini, G.; Jalil, R.; Bonini, N.; Basko, D. M.; Galiotis, C.; Marzari, N.; Novoselov, K. S.; Geim, A. K.; Ferrari, A. C. Uniaxial strain in graphene by Raman spectroscopy: G peak splitting, Grüneisen parameters, and sample orientation. *Phys. Rev. B: Condens. Matter Mater. Phys.* **2009**, *79* (20), 205433.

(14) Ferrari, A. C.; Robertson, J. Interpretation of Raman spectra of disordered and amorphous carbon. *Phys. Rev. B: Condens. Matter Mater. Phys.* **2000**, *61* (20), 14095.

(15) Cancado, L. G.; Jorio, A.; Ferreira, E. H.; Stavale, F.; Achete, C. A.; Capaz, R. B.; Moutinho, M. V.; Lombardo, A.; Kulmala, T. S.; Ferrari, A. C. Quantifying defects in graphene via Raman spectroscopy at different excitation energies. *Nano Lett.* **2011**, *11* (8), 3190−3196.

(16) Bruno, G.; Capezzuto, P.; Bianco, G. V. The pivotal role of plasmachemistry in determining a sustainable future for graphene innovations. *Rendiconti Lincei. Scienze Fisiche e Naturali* **2019**, *30* (3), 563−572.

(17) Luo, Z.; Yu, T.; Kim, K.-j.; Ni, Z.; You, Y.; Lim, S.; Shen, Z.; Wang, S.; Lin, J. Thickness-dependent reversible hydrogenation of graphene layers. *ACS Nano* **2009**, *3* (7), 1781−1788.

(18) Eckmann, A.; Felten, A.; Mishchenko, A.; Britnell, L.; Krupke, R.; Novoselov, K. S.; Casiraghi, C. Probing the nature of defects in graphene by Raman spectroscopy. *Nano Lett.* **2012**, *12* (8), 3925−3930.

(19) Blankenburg, S.; Bieri, M.; Fasel, R.; Mullen, K.; Pignedoli, C. A.; Passerone, D. Porous graphene as an atmospheric nanofilter. *Small* **2010**, *6* (20), 2266−2271.

(20) Sun, P. Z.; Yang, Q.; Kuang, W. J.; Stebunov, Y. V.; Xiong, W. Q.; Yu, J.; Nair, R. R.; Katsnelson, M. I.; Yuan, S. J.; Grigorieva, I. V.; Lozada-Hidalgo, M.; Wang, F. C.; Geim, A. K. Limits on gas impermeability of graphene. *Nature* **2020**, *579* (7798), 229−232.

Supporting Information

Selective gas permeation in defect-engineered bilayer graphene

Jiaman Liu[1,2], Lei Jin[2,3], Frances I. Allen[2,4], Yang Gao[2,5], Penghong Ci[2,3], Feiyu Kang[1,6,7]*, Junqiao Wu[2,3]*

[1]Environmental Science and New Energy Technology Engineering Laboratory, Shenzhen Geim Graphene Center (SGGC) and Tsinghua-Berkeley Shenzhen Institute (TBSI), Tsinghua University, Shenzhen 518055, China.
[2]Department of Materials Science and Engineering, University of California, Berkeley, California 94720, United States.
[3]Materials Sciences Division, Lawrence Berkeley National Laboratory, Berkeley, California 94720, United States.
[4]National Center for Electron Microscopy, Molecular Foundry, Lawrence Berkeley National Laboratory, Berkeley, California 94720, USA.
[5]Department of engineering mechanics, Zhejiang University, Hangzhou 310027, China
[6]Institute of Materials Research and Shenzhen Geim Graphene Center (SGGC), Shenzhen International Graduate School (SIGS), Tsinghua University, Shenzhen 518055, China.
[7]Laboratory of Advanced Materials, School of Materials Science and Engineering, Tsinghua University, Beijing 100084, China.
*E-mail: fykang@sz.tsinghua.edu.cn
*E-mail: wuj@berkeley.edu

EXPERIMENT SECTION

Micro-cavity wafer fabrication. Photolithography and reactive ion etching were used to obtain disk-shaped holes with depths of 400-1000 nm in an oxidized silicon wafer with 300 nm silicon oxide on top. The hole diameters were 5 μm. After the holes were fabricated the wafer was cut into chips (around 1 cm×1cm). The chips were then ultrasonically-cleaned in acetone and IPA, for 10 minutes in each case, and finally dried with N_2 gas flow to remove particles and organic contaminants adsorbed on the surface. Prior to graphene exfoliation, oxygen plasma treatment (120 W, 20 sccm H_2, 3 min) was used to further react with remnant hydrocarbons and contaminants adsorbed on the surface and help increase the adhesion between the graphene and the substrate.

Graphene transfer. Immediately after the oxygen plasma treatment, graphite flakes (NGS Naturgraphit GmbH) mechanically-thinned by repeated scotch-tape exfoliation were pressed onto the chip. Additional pressure was gently applied to the tape adhered to the chip using a soft-tipped tweezer. The chip was then heated at 80˚C for ~1 minute on a hot plate to further increase the adhesion. After cooling to room temperature, the tape was slowly peeled off to leave the graphene flakes on the chip. Optical microscopy was used to identify bilayer graphene (BLG) flakes, whereby the underlying SiO_2 layer produced contrast up to 12% to make the graphene visible[1].

He$^+$ ion irradiation. A He$^+$ ion microscope (Zeiss Orion NanoFab) equipped with a pattern generator (NPVE from Fibics, Inc.) and operated at 30 keV with probe currents ranging from 0.05 to 0.25 pA (10 μm aperture, spot control 5-6, helium pressure at source 2×10^6 Torr) was used to irradiate the graphene under an angle of incidence of 90˚. For each ion dose, a dwell time of 1 μs and irradiation spot spacing of 0.25 nm was used, which ensures continuity of irradiation over the BLG surfaces (the He$^+$ beam diameter is ~0.5 nm). As the BLG was suspended over a 5 μm-diameter micro-cavity, the irradiated region was slightly larger (*i.e.* 6 μm in diameter) to cover the entire suspended region.

H_2 plasma treatment. Hydrogen plasma treatment of the graphene was conducted in a plasma-enhanced chemical vapor deposition chamber using the Oxford Plasmalab System 100 (capacitively-coupled type). The plasma treatment was conducted using radio frequency (13.56 MHz), at 350˚C, 1 Torr, and 20 W, for different time periods.

Pressurization chamber. The as-exfoliated graphene samples on the micro-cavity substrate were placed into a home-built pressurized chamber. After repeated inflating (in each test gas) and deflating (in vacuum) for three times, the chamber was re-pressurized with N_2, H_2, He, and CH_4 using charging pressures of ~3000 Torr, ~2000 Torr, ~3000 Torr, and ~3000 Torr, respectively.

AFM measurement. AFM images were obtained in tapping mode using a Veeco Multi-mode AFM.

Raman measurement. Raman spectroscopy was conducted using a Renishaw confocal micro-Raman microscope with a laser excitation wavelength of 488 nm, a 100× objective (NA=0.95) (laser spot size is ~1 μm), and a 2400 g/mm grating. The acquisition time was 10 s and the laser power was set to ~1 mW in order to minimize sample damage.

NOTE S1

According to Ferrari *et al.*[2], in stage 1, *i.e.*, the graphite transforming to nanocrystalline graphite, and the D and D' peak appear and I_D/I_G increases with all peaks broadened. In stage 2, *i.e.*, nanocrystalline graphite transforming to low sp^3 amorphous carbon, the G peak position decreases and I_D/I_G decreases toward 0. In stage 3, *i.e.*, low sp^3 amorphous carbon transforming to high sp^3 (tetrahedrally-coordinated) amorphous carbon, the G peak position increases and I_D/I_G is very low or nearly 0.

NOTE S2

For a clamped circular membrane, the molecular flux, dn/dt, leaking out of the over-pressurized 'blister' can be derived using the ideal gas law and Hencky's solution[3],

$$\frac{dn}{dt} = \frac{\left[\frac{3K(\nu)(Ew\delta^2)}{a^4} \cdot V(\delta) + \pi a^2 C(\nu)P_{atm}\right]}{RT}\frac{d\delta}{dt},$$

where *n* is the number of moles of gas molecules sealed in the micro-cavity, *t* is time, *E* is Young's modulus, ν is Poisson's ratio, w is the thickness, of the membrane, $K(\nu)$ is a coefficient that depends on ν, R is the gas constant, T is temperature, $V(\delta)$ is the total volume of the sealed gas molecules when the membrane is bulged with deflection δ, $V(\delta) = V_0 + V_b(\delta)$, $V_0 = \pi a^2 \cdot h$ is the volume of the disk-shaped micro-cavity, h is the depth of the micro-cavity, $V_b(\delta) = C(\nu)\pi a^2\delta$, $C(\nu = 0.16) = 0.52$ is a coefficient that depends only on ν, P_{atm} is the atmospheric pressure, a_0 is the diameter of the circular cavity, and a is the diameter of the bulged membrane.

Figure S1. Optical image of BLG exfoliated onto an SiO_2(300nm)/Si wafer with pre-etched holes.
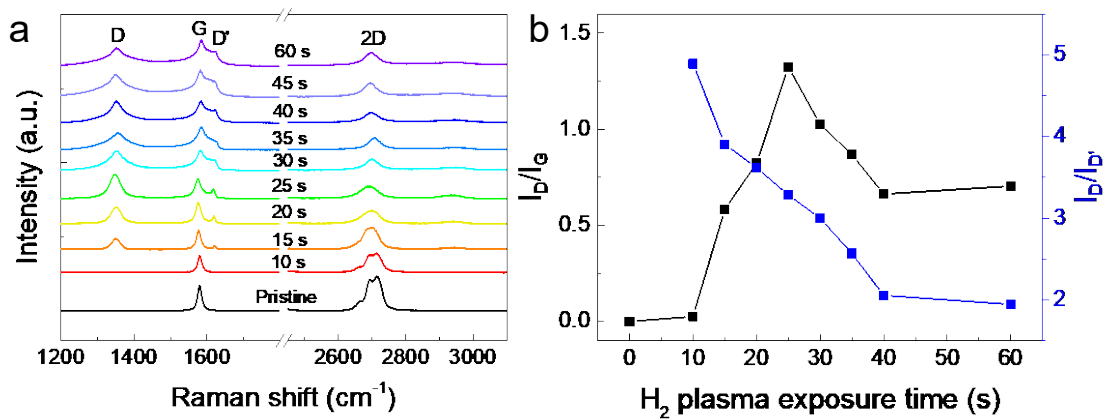
Figure S2. a, Evolution of 2D, D', G, and D Raman peaks as a function of H_2 plasma exposure time. b, Corresponding evolution of I_D/I_G and $I_D/I_{D'}$ versus plasma exposure time.
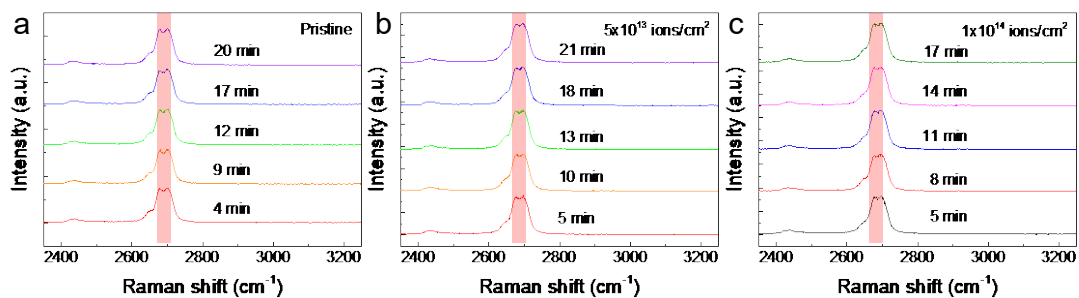
Figure S3. Evolution of Raman spectra for: a, Pristine BLG balloon, b) ion-irradiated BLG balloon using 5×10^{13} ions/cm^2, and c, ion-irradiated BLG balloon using 1×10^{14} ions/cm^2 dose, for different time points upon deflation.
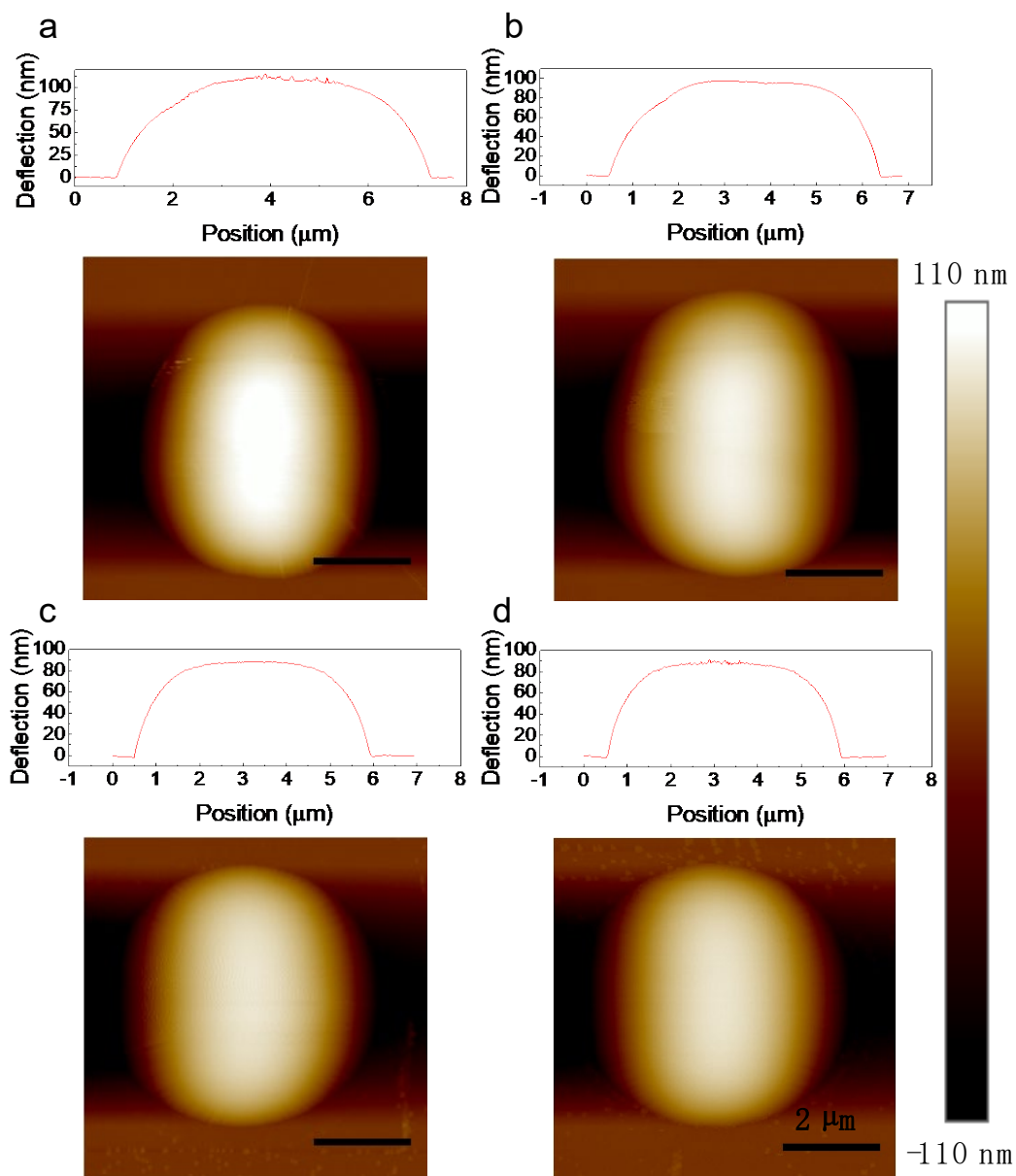
Figure S4. AFM images of a BLG balloon showing different deflections after removal from the pressure chamber: a, 109 nm, b, 96 nm, c, 90 nm, and d, 90 nm.
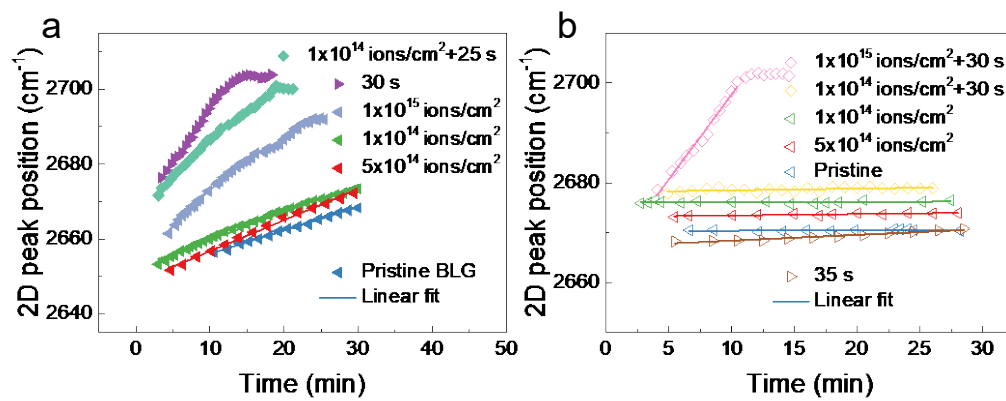
Figure S5. a, He permeance results and b, CH_4 permeance results.

Tabls S1. Experimental values for L_D and n_D calculated from Raman spectra for different irradiation doses.

Irradiation dose (ions/cm²)	L_D (nm)	n_D (cm^{-2})
5×10^{13}	17.17	1.08×10^{11}
1×10^{14}	13.46	1.76×10^{11}
3×10^{14}	9.20	3.76×10^{11}
5×10^{14}	8.08	4.88×10^{11}
7×10^{14}	7.37	5.86×10^{11}
1×10^{15}	6.92	6.65×10^{11}
2×10^{15}	6.60	7.30×10^{11}
3×10^{15}	6.55	7.43×10^{11}
4×10^{15}	3.15	3.21×10^{12}
5×10^{15}	3.02	3.49×10^{12}

Table S2. N$_2$ leak rates extracted from the measured Raman peak position shift rates.

Sample	2D peak shift rate (cm^{-1}/min)	Deflection shift rate, $d\delta/dt$ (nm/s)	Maximum deflection, δ (nm)	Radius, a (µm)	Molecular flux, dn/dt (mol/s)	Normalized dn/dt (mol/s·Pa)	Leak rate (mol/s·m²·Pa)
Pristine BLG	0.0125	0.00056	100	5.8	1.50×10^{-21}	5.01×10^{-27}	4.74×10^{-17}
1×10^{14} ions/cm^2	0.0141	0.00064	100	5.8	1.69×10^{-21}	5.65×10^{-27}	5.35×10^{-17}
5×10^{14} ions/cm^2	0.0129	0.00058	100	5.8	1.55×10^{-21}	5.17×10^{-27}	4.89×10^{-17}
30 s	0.0166	0.00075	100	5.8	1.99×10^{-21}	6.65×10^{-27}	6.29×10^{-17}
35 s	0.1156	0.00521	100	5.8	1.39×10^{-20}	4.63×10^{-26}	4.38×10^{-16}
40 s	9.8100	0.44189	100	5.8	1.18×10^{-18}	3.93×10^{-24}	3.72×10^{-14}
1×10^{14} ions/cm^2 +30 s	0.0534	0.00241	100	5.8	6.40×10^{-21}	2.14×10^{-26}	2.02×10^{-16}
1×10^{15} ions/cm^2 +30 s	7.1028	0.31995	100	5.8	8.51×10^{-19}	2.85×10^{-24}	2.69×10^{-14}
3×10^{14} ions/cm^2 +35 s	30.7308	1.38427	100	5.8	3.68×10^{-18}	1.23×10^{-23}	1.16×10^{-13}

Table S3. H_2 leak rates extracted from the measured Raman peak position shift rates.

Sample	2D peak shift rate (cm^{-1}/min)	Deflection shift rate, $d\delta/dt$ (nm/s)	Maximum deflection, δ (nm)	Radius, a (μm)	Molecular flux, dn/dt (mol/s)	Normalized dn/dt (mol/s·Pa)	Leak rate (mol/s·m^2·Pa)
Pristine BLG	0.04	0.0018	100	5.8	4.79×10^{-21}	2.88×10^{-26}	2.73×10^{-16}
1×10^{14} ions/cm^2	0.09	0.0041	100	5.8	1.08×10^{-20}	6.49×10^{-26}	6.14×10^{-16}
5×10^{14} ions/cm^2	0.15	0.0068	100	5.8	1.80×10^{-20}	1.08×10^{-25}	1.02×10^{-15}
1×10^{15} ions/cm^2	3.68	0.1658	100	5.8	4.41×10^{-19}	2.65×10^{-24}	2.51×10^{-14}
30 s	0.06	0.0027	100	5.8	7.19×10^{-21}	4.33×10^{-26}	4.10×10^{-16}
35 s	7.28	0.3279	100	5.8	8.73×10^{-19}	5.25×10^{-24}	4.97×10^{-14}
1×10^{14} ions/cm^2 +25 s	0.05	0.0023	100	5.8	5.99×10^{-22}	3.60×10^{-26}	3.41×10^{-16}
1×10^{14} ions/cm^2 +30 s	14.67	0.6608	100	5.8	1.76×10^{-18}	1.06×10^{-23}	1.00×10^{-13}
1×10^{15} ions/cm^2 +30 s	14.00	0.6306	100	5.8	1.68×10^{-18}	1.01×10^{-23}	9.56×10^{-14}

Table S4. He leak rates extracted from the measured Raman peak position shift rates.

Sample	2D peak shift rate (cm^{-1}/min)	Deflection shift rate, $d\delta/dt$ (nm/s)	Maximum deflection, δ (nm)	Radius, a (μm)	Molecular flux, dn/dt (mol/s)	Normalized dn/dt (mol/s·Pa)	Leak rate (mol/s·m^2·Pa)
Pristine BLG	0.62	0.0279	100	5.8	7.431×10^{-20}	2.48×10^{-25}	2.35×10^{-15}
1×10^{14} ions/cm^2	0.73	0.0329	100	5.8	8.75×10^{-20}	2.92×10^{-25}	2.77×10^{-15}
3×10^{14} ions/cm^2	0.77	0.0347	100	5.8	9.23×10^{-20}	3.08×10^{-25}	2.92×10^{-15}
5×10^{14} ions/cm^2	0.82	0.0369	100	5.8	9.83×10^{-20}	3.28×10^{-25}	3.11×10^{-15}
7×10^{14} ions/cm^2	0.99	0.0446	100	5.8	1.19×10^{-19}	3.97×10^{-25}	3.75×10^{-15}
1×10^{15} ions/cm^2	1.78	0.0802	100	5.8	2.13×10^{-19}	7.13×10^{-25}	6.75×10^{-15}
30 s	2.71	0.1221	100	5.8	3.25×10^{-19}	1.09×10^{-24}	1.03×10^{-14}
1×10^{14} ions/cm^2 +25s	1.99	0.0896	100	5.8	2.39×10^{-19}	7.97×10^{-25}	7.55×10^{-15}

Table S5. CH_4 leak rates extracted from the measured Raman peak position shift rates.

Sample	2D peak shift rate (cm^{-1}/min)	Deflection shift rate, $d\delta/dt$ (nm/s)	Maximum deflection, δ (nm)	Radius, a (μm)	Molecular flux, dn/dt (mol/s)	Normalized dn/dt (mol/s·Pa)	Leak rate (mol/s·m^2·Pa)
Pristine BLG	0.01	0.0005	100	5.8	1.20×10^{-21}	4.01×10^{-27}	3.79×10^{-17}
1×10^{14} ions/cm^2	0.01	0.0005	100	5.8	1.20×10^{-21}	4.01×10^{-27}	3.79×10^{-17}
5×10^{14} ions/cm^2	0.02	0.0009	100	5.8	2.40×10^{-21}	8.01×10^{-27}	7.58×10^{-17}
35 s	0.12	0.0054	100	5.8	1.44×10^{-20}	4.81×10^{-26}	4.55×10^{-16}
1×10^{14} ions/cm^2 +30 s	0.03	0.0014	100	5.8	3.60×10^{-21}	1.20×10^{-26}	1.14×10^{-16}
1×10^{15} ions/cm^2 +30 s	3.40	0.1532	100	5.8	4.08×10^{-19}	1.36×10^{-24}	1.29×10^{-14}

REFERENCES

(1)	Blake, P.; Hill, E. W.; Castro Neto, A. H.; Novoselov, K. S.; Jiang, D.; Yang, R.; Booth, T. J.; Geim, A. K. Making graphene visible. *Appl. Phys. Lett.* **2007,** 91 (6), 063124.

(2)	Ferrari, A. C.; Robertson, J. Interpretation of Raman spectra of disordered and amorphous carbon. *Phys. Rev. B* **2000,** 61 (20), 14095.

(3)	Koenig, S. P.; Wang, L.; Pellegrino, J.; Bunch, J. S. Selective molecular sieving through porous graphene. *Nat. Nanotechnol.* **2012,** 7 (11), 728‐732.